Visual Informatics 9 (2025) 58–70

Contents lists available at ScienceDirect

Visual Informatics

journal homepage: www.elsevier.com/locate/visinf

Research article

# Key-isovalue selection and hierarchical exploration visualization of weather forecast ensembles

Feng Zhou, Hao Hu, Fengjie Wang, Jiamin Zhu, Wenwen Gao, Min Zhu *

*College of Computer Science, Sichuan University, China*

ARTICLE INFO

*Article history:*
Received 26 January 2024
Received in revised form 28 January 2025
Accepted 3 February 2025
Available online 5 February 2025

*Keywords:*
Ensemble visualization
Isocontours
Hierarchical visualization
Isovalue selection
Spaghetti plots

ABSTRACT

Weather forecast ensembles are commonly used to assess the uncertainty and confidence of weather predictions. Conventional methods in meteorology often employ ensemble mean and standard deviation plots, as well as spaghetti plots, to visualize ensemble data. However, these methods suffer from significant information loss and visual clutter. In this paper, we propose a new approach for uncertainty visualization of weather forecast ensembles, including isovalue selection based on information loss and hierarchical visualization that integrates visual abstraction and detail preservation. Our approach uses non-uniform downsampling to select key-isovalues and provides an interactive visualization method based on hierarchical clustering. Firstly, we sample key-isovalues by contour probability similarity and determine the optimal sampling number using an information loss curve. Then, the corresponding isocontours are presented to guide users in selecting key-isovalues. Once the isovalue is chosen, we perform agglomerative hierarchical clustering on the isocontours based on signed distance fields and generate visual abstractions for each isocontour cluster to avoid visual clutter. We link a bubble tree to the visual abstractions to explore the details of isocontour clusters at different levels. We demonstrate the utility of our approach through two case studies with meteorological experts on real-world data. We further validate its effectiveness by quantitatively assessing information loss and visual clutter. Additionally, we confirm its usability through expert evaluation.



## 1. Introduction

Ensemble forecasting involves generating multiple weather predictions (i.e., ensemble members) to represent various possible future atmospheric states (Leutbecher and Palmer, 2008). This is achieved by utilizing different mathematical prediction models, perturbed initial conditions, varying spatial resolutions, or different vertical coordinate systems (Ferstl et al., 2017; De Souza et al., 2023). These ensemble members provide valuable information about the probability distribution of forecasted fields, which aids in assessing weather variability. Over the past decades, ensemble forecasting has become widely used for evaluating the reliability of weather predictions. Given the extensive scale and high complexity of ensemble forecast data, visualization plays a crucial role in effectively conveying the uncertainty and confidence associated with these predictions (Ma and Entezari, 2019; Liu et al., 2019; Kumpf et al., 2019; Kamal et al., 2021).

Since ensemble isocontours of different isovalues exhibit different variability behaviors, it is essential to select interesting isovalues that provide the most useful information for subsequent specific isocontour analysis (Wang, 2020). The conventional method for isovalue selection in weather forecasting relies on the utilization of the ensemble mean and standard deviation plot. This plot employs the contours of the ensemble mean as a representation of the ensemble and maps the standard deviation of each grid point to a gradient background color (Sanyal et al., 2010). However, the standard deviation could be misleading for regions with large gradients, since small displacements of members can lead to a large standard deviation. Alternatively, several studies assisted users in selecting isovalue by extracting a limited number of representative isocontour samples (Ma and Entezari, 2019; Zhang et al., 2021). However, these approaches have not taken into account the controllability of the information loss between the sampled results and the original ensemble, resulting in the possibility of missing key contour structures.

Once the isocontour of interest has been chosen, the attention shifts towards examining the variability of isocontours. A commonly employed technique for this purpose is the spaghetti plot. This technique involves overlaying the isocontours of each ensemble member onto a single view, all based on the same isovalue (Rautenhaus et al., 2018). It invariably results in visual clutter when dealing with a large size of ensemble members, making it challenging for observers to distinguish between isocontours

* Corresponding author.
*E-mail addresses:* zhoufeng@stu.scu.edu.cn (F. Zhou), zhumin@scu.edu.cn (M. Zhu).

https://doi.org/10.1016/j.visinf.2025.02.001

of different members (Ma and Entezari, 2019). Therefore, in recent years, there have been efforts to improve spaghetti plots and explore visual abstraction. Sanyal et al. (2010) quantified ensemble uncertainty by utilizing member standard deviation, inter-quartile range, and the width of the 95% confidence interval. They then represented these measures using gradient-colored circular glyphs. Ferstl et al. (2016b) performed clustering analysis on ensemble isocontours and introduced confidence bands based on signed distance functions to convey the major trends and outliers in a set of isocontours. These methods reduce the visual clutter of spaghetti plots while providing a summary of the variability information. However, they sacrifice the capability to directly examine the original isocontours and entail the loss of details within the isocontours (Viola et al., 2020). Striking a balance between managing visual clutter and preserving important details poses an urgent problem that requires attention.

Several attempts have been made to address the above situations. The work conducted by Ma and Entezari (2019) may be the closest to ours. They performed clustering on the ensemble isocontours of each isovalue and displayed top-ranked isocontours of all significant hierarchies to guide meteorological experts in selecting isovalues for visual analysis. However, they did not downsample the value range of isovalues to identify key-isovalues with representative contour structures, nor did they take into account the potential impact of information loss. In terms of hierarchical exploration, they generalized the high-density clustering for isocontours, representing the hierarchy of the density function as a hierarchy of nested subsets of the ensemble data. This hierarchy was then visualized as a mode plot linked with spaghetti plots. Nonetheless, the mode plot not only failed to provide an overview of the hierarchy, but it also did not allow users to flexibly switch between the overview and any cluster level to explore detailed information about the ensemble isocontours. Additionally, the linked spaghetti plots did not integrate the confidence band, and only performed filtering and display of isocontours, resulting in poor performance when many isocontours need to be displayed.

To address these issues, we propose a novel approach for key-isovalue selection guided by contours and hierarchical exploration of isocontour clusters in weather forecast ensembles. Our approach enables a comprehensive analysis process of ensemble isocontours, from the key-isovalue selection that controls information loss to the isocontour band visualization that reduces visual clutter. Our approach first extracts representative isocontours through non-uniform downsampling and calculates the information loss under different sampling numbers to determine the optimal sampling number. This ensures controllable information loss. Leveraging the displayed key contour structures, variability range of contours, and their spatial distribution, our approach offers guidance for selecting the desired isovalue. Once the isovalue is selected, our method performs hierarchical clustering on ensemble isocontours, allowing for interactive customization of the clustering hierarchy to account for the varying dispersion of the ensemble data at different time-steps. To reduce visual clutter, we construct a visualization of isocontour clusters, the isocontour bands, and employ an interactive bubble tree to depict the hierarchical structure of the clusters. This enables hierarchical exploration of isocontour clusters. To evaluate the utility, effectiveness, and usability of our approach, we conduct case studies using real-world data. We also perform quantitative assessments of information loss and visual clutter. Additionally, we conduct interviews with domain experts. The results demonstrate that our approach effectively guides the key-isovalue selection while preserving the essential information of the original ensemble isocontours. It also facilitates interactive hierarchical exploration of isocontour clusters with less visual clutter, assisting meteorological experts in intuitively exploring and analyzing the uncertainty and confidence of ensemble data.

The contributions of this paper include:

- Key-isovalue selection guided by contours: We propose a non-uniform downsampling approach based on contour probability similarity to assist users in selecting representative isocontours. We utilize contour probability to represent the uncertainty of isocontours and assess representativeness based on differences in probability distributions. We quantify the information loss caused by sampling and make it controllable by automatically determining the optimal sampling number through the information loss curve.
- Hierarchical exploration of isocontour clusters: We reduce visual clutter caused by the increasing size of ensemble members through the visual abstraction of isocontour clusters. We link a bubble tree that represents the clustering hierarchy to the visual abstraction, allowing for interactive and flexible switching between different levels of detail when observing isocontours. We enable customization of the hierarchical structure to present ensemble isocontours at different dispersions.

## 2. Related work

The multivalued nature of ensemble data, generated by various prediction models with different settings, introduces inherent uncertainty, making ensemble visualization a specific category within uncertainty visualization (Kamal et al., 2021). In recent years, ensemble visualization has gained significant traction in meteorology (Rautenhaus et al., 2018), playing a pivotal role in assisting meteorological experts to develop a more intuitive understanding of ensemble weather forecasts (Wang et al., 2019). Obermaier and Joy (2014) classified ensemble visualization into two main categories: feature-based and location-based methods. Our approach is a feature-based method that focuses on isocontours in scalar fields. We extract features (i.e., isocontours) from individual ensemble members and compare them across the ensemble. In this section, we provide a comprehensive review of the most relevant literature to our work.

Isocontour is a crucial feature in 2D scalar fields, allowing researchers to represent the uncertainty and confidence of ensembles of scalar fields by showcasing the contour structure and variation range of the isocontours. The spaghetti plot is the only conventional visualization technique that directly examines the isocontour distribution behavior of all ensemble members (Quinan and Meyer, 2016). Plotting isocontours for all ensemble members on a single plane leads to significant visual clutter, making spaghetti plots challenging to parse (Ma and Entezari, 2019). To improve spaghetti plots, Pfaffelmoser and Westermann (2012) employed a special background and foreground color mapping strategy to enhance the observer's capability to differentiate topological differences in isocontours with different trends. However, this method is only effective for a small number of trends and still suffers from visual clutter interference. An alternative approach is to utilize the visual abstraction technique. For example, Sanyal et al. (2010) employed gradient-colored circular glyphs to encode the statistical distribution of the ensemble at various locations in the spatial domain and created an abstract contour band visualization by placing these glyphs along the isocontours of the ensemble mean. While this method can depict the summarization of confidence regions for isocontours, it sacrifices the detailed geometric information of individual isocontours by relying solely on the ensemble mean.

Subsequent research has further explored the visual abstraction technique. Whitaker et al. (2013) introduced the concept of contour boxplots, which extend different types of confidence band regions based on statistical band depth to demonstrate the variability of isocontours. Mirzargar et al. (2014) further extended this approach to visualize curve sets such as streamlines and trajectories. Ferstl et al. (2016b) developed contour variability plots, which treat the signed distance field of the isocontours as data points in high-dimensional space and generate statistical confidence ellipses. They then map the mean and standard deviation back to the contour cluster band for visualization. Kumpf et al. (2018) designed contour probability plots, which calculate the percentage of ensemble members above a set isovalue at each point in the scalar field, resulting in a contour band visualization with more confidence intervals. Building upon these previous studies, Zhang et al. (2023) proposed a unified framework of ensemble contour visualization, incorporating member filtering, point-wise modeling, uncertainty band extraction, and visual mapping. These approaches effectively reduce visual clutter through visual abstraction and convey the major trends, outliers, and other variability information of ensemble isocontours in terms of geometric shape and spatial location. However, it is important to note that visual abstraction comes at the cost of losing detailed information (Viola et al., 2020). To address this issue, our approach links a bubble tree to visual abstractions to explore detailed information about isocontour bands or original isocontours at different levels of hierarchy.

While previous research on visualizing ensemble isocontours has typically assumed that expert users possess prior knowledge of the isovalues of interest and then analyze the extracted isocontours (Ferstl et al., 2017; Sanyal et al., 2010; Ferstl et al., 2016b; Quinan and Meyer, 2016; Whitaker et al., 2013; Kumpf et al., 2018; Zhang et al., 2023), it may not be the case. Thus, studies are conducted to guide users in selecting interesting isovalues based on the numerical distribution and contour features of the ensemble data. Sanyal et al. (2010) utilized ensemble mean and standard deviation plots to assist users in clicking on points of interest and selecting the isovalues corresponding to the ensemble mean at those points. However, the point-wise computed standard deviation may not fully reflect the variability of the ensemble isocontours (Zhang et al., 2021). Hazarika et al. (2018) calculated the predictability and surprise of individual isovalues based on conditional entropy and visualized it in a scatter plot, but representing the original contours as scatter points may lack intuitiveness. Some other studies guide users in isovlaue selection by filtering and displaying a small number of representative isocontours. Ma and Entezari (2019) clustered the ensemble isocontours corresponding to each isovalue and selected all significant mode samples for display, while Zhang et al. (2021) selected a few isovalues based on their proposed variable spatial spreading for visualization. However, these methods do not assess the representativeness of the selected small samples across all possible isovalues, which can lead to the omission of key contour structures (i.e., the loss of important information), potentially affecting the subsequent analysis process. In contrast, our approach applies the range likelihood field, proposed by He et al. (2017), to calculate contour probability similarity, which we use to prioritize isovalue selection. Based on this, we perform non-uniform downsampling to obtain key-isovalues and calculate the information loss for different sampling numbers, thereby assessing the representativeness of the selected samples. In this regard, we argue that our method advances the process by guiding users in selecting key-isovalues with consideration of information loss.

To sum up, we focus on the information loss in isovalue selection and the visual clutter in contour visualization. We design a visual analysis method to support guided isovalue selection and interactive visual exploration of weather forecast ensembles.

## 3. Method overview

During the design process of this paper, we conduct interviews with three experts (P1–P3) from the meteorological administration over five months. P1, a forecaster with 11 years of experience, and P2 and P3, meteorologists specializing in ensemble forecasting for 14 and 22 years, respectively. Throughout the design process, we conducted regular half-monthly meetings with the experts, where we presented them with the latest ideas and design details for their feedback on potential enhancements, which have significantly contributed to our work. The workflow and visualization provided by our approach are illustrated in Fig. 2. Next, we provide a high-level description of our method.

Our approach starts with an ensemble $s_1^{[1:T]}, \ldots, s_N^{[1:T]} \in \mathbb{R}^{M \times T}$ of $N$ 2D time-dependent scalar forecast fields, representing the evolving weather states over $T$ time-steps. Subscripts and superscripts, respectively, denote the ensemble member and time-step. All ensemble members are defined on the same grid structure, e.g., longitude-latitude grid, with $M$ grid points. For a prescribed forecast time-step $t$, the subsets $s_1^t, \ldots, s_N^t \in \mathbb{R}^M$ are treated as $N$ single elements as illustrated in Fig. 2(a).

The value range of subsets $s_1^t, \ldots, s_N^t$ is divided into $L$ intervals equidistantly, and $L$ contour probabilities (Fig. 2(b2)) corresponding to each interval isovalue are extracted using kernel density estimation (Fig. 2(b1)). To reduce visual clutter, downsampling (Fig. 2(b4)) is then performed based on the similarity (Fig. 2(b3)) between these $L$ contour probabilities. This process selects $S$ key-isovalues that possess distinctive and representative contour structures. The optimal sampling number, $S$, is automatically determined based on the information loss incurred during downsampling. Subsequently, the ensemble isocontours corresponding to the $S$ key-isovalues are obtained and used to construct a spaghetti plot set as illustrated in Fig. 2(b5). To avoid overlap and interference among the isocontours of adjacent isovalues, we control the number of spaghetti plots according to $S$, conveying intuitive visual information to users and providing guidance for their selection of isovalues.

After the selection of isovalues, we proceed to extract the signed distance fields (Fig. 2(c1)) for each ensemble member. Considering computation speed, we employ agglomerative hierarchical clustering (Fig. 2(c2)) to construct a hierarchical cluster tree. To address the dispersion of ensemble isocontours increase as the forecast time progresses (Leutbecher and Palmer, 2008), as well as to simplify the hierarchical exploration of isocontour clusters (Fig. 2(c3)), we provide users with the flexibility to customize the number of leaf node clusters and the number of branches per level. Then, we generate visual abstractions for each cluster of different levels. By merging the signed distance fields of each member of the cluster, we obtain abstract isocontour bands that provide a summarized visualization. These isocontour bands depict the spatial distribution range and the variability information of the isocontours within each cluster, including their mean, standard deviation, and spatial position. Additionally, we utilize a bubble tree to represent the hierarchical structure of the clusters, which is linked to the isocontour bands, as illustrated in Fig. 2(c4). Users can navigate between different cluster levels by interacting with the bubble tree, and the isocontour bands at varying levels will be reconstructed and presented accordingly.

Fig. 1 shows a screenshot of the method in use. Users can interactively modify the forecast time-step, the number of ensemble members, and the geographical region for re-analysis within the main interface. Furthermore, users can add multiple sub-interfaces for key-isovalue selection and hierarchical exploration of isocontours. To facilitate precise coordinate selection for any geographical point, synchronized latitude and longitude coordinate pickers are available in multiple views, as illustrated in Fig. 3.

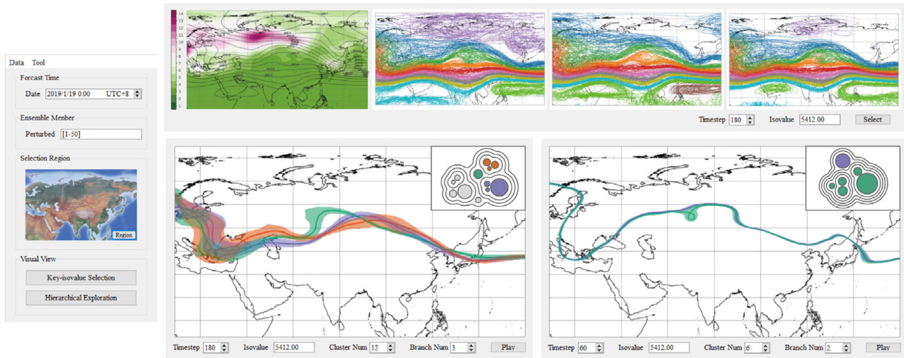


**Fig. 1.** Key-isovalue Selection and Hierarchical Exploration Visualization of Weather Forecast Ensembles: After determining the basic parameters (left), users can select isovalue based on the downsampled isocontours (top right). The hierarchical information of isocontour clusters extracted from the selected key-isovalue is displayed as a bubble tree and can be interactively explored with the isocontour bands (bottom middle). Users can customize the hierarchical structure parameters for isocontour clusters with different dispersions (bottom right).

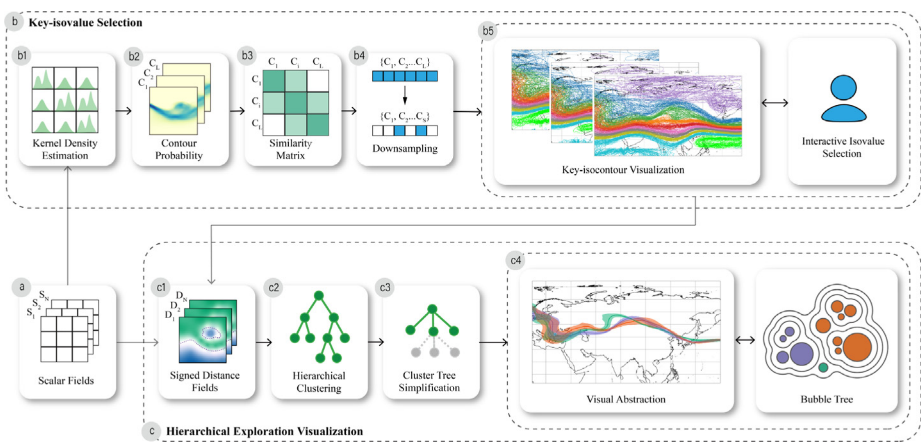


**Fig. 2.** Method overview. (a) Scalar forecast field ensembles. (b) Kernel density estimation of weather forecast ensembles, extraction of contour probability, downsampling based on the dissimilarity matrix, and visualization of the sampling results to assist users in selecting the corresponding key-isovalue. (c) Extraction of signed distance fields based on the selected isovalue, hierarchical clustering of the ensemble members, simplification of the hierarchical cluster tree, and hierarchical exploration of isocontour clusters by linking the bubble tree to the isocontour bands.

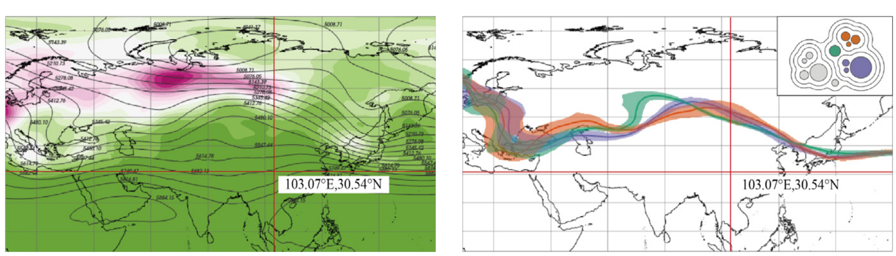


(a) (b)

**Fig. 3.** Latitude and longitude coordinate pickers with linked displays between different views.

## 4. Key-isovalue selection

To obtain representative isocontours from ensemble data, it is a conventional practice to employ downsampling techniques considering the variability features (Liu et al., 2017). However, a higher sampling number may lead to substantial overlap among different isocontours, thereby reducing selection efficiency. Conversely, reducing the sampling number may result in the omission of key contour structures, consequently increasing information loss. To strike a balance between selection efficiency and information preservation, we propose a new approach for key-isovalue selection based on the downsampling of contour probability as illustrated in Fig. 2(b).

In the following, we describe the calculation for the similarity between contour probabilities extracted for each isovalue (Section 4.1). This similarity serves as a measure of the degree to which the contour structure of one isovalue can be represented by the contour structure of other isovalues. By leveraging this similarity, we implement a downsampling technique for selecting key-isovalues (Section 4.2). To ensure that no significant contour structures are missed, we evaluate the information loss across various sampling results and determine the optimal sampling number to be taken (Section 4.3). We then visualize the ensemble isocontours corresponding to the final selected key-isovalues (Section 4.4).

### 4.1. Calculation of contour probability similarity

Inspired by the studies of He et al. (2017) and Pothkow and Hege (2011), we commence by extracting the contour probabilities associated with each isovalue to analyze the similarity among various isovalues within a set of scalar fields. For a prescribed forecast time-step $t$, given a set of 2D scalar forecast fields $s_1^t, \ldots, s_N^t \in \mathbb{R}^M$, and for any grid point $g$ with scalar values $x = \{x_1, \ldots, x_N\}$ obtained from different ensemble members, we employ the following function to perform kernel density estimation:

$$f_h(g; x) = \frac{1}{Nh} \sum_{i=1}^{N} K\left(\frac{x - x_i}{h}\right)$$

where $K$ is a smooth function called the kernel function, and in this case, we use the standard normal distribution. For the bandwidth $h$ which governs the level of smoothness, we follow the research recommendation by Pöthkow and Hege (2013) and employ Silverman's rule of thumb as an automatic bandwidth selection strategy.

Given $L$ equidistant intervals $\Gamma_1, \Gamma_2, \ldots, \Gamma_L$ that partition the value range of the scalar field, we designate the median of each interval as a candidate isovalue. For each interval $\Gamma_i, i = 1, \ldots, L$, the cumulative probability value at each grid point $g$ is calculated by the range likelihood field as

$$L_X\left(g; \Gamma_i\right) = \int_{\Gamma_i} f_X(g; x) dx.$$

We obtain a set of contour probabilities $c_1, \ldots, c_L \in \mathbb{R}^M$, each of which forms a scalar field. In this scalar field, each grid point is assigned a scalar value, which indicates the probability of ensemble isocontours passing through that specific point for a given isovalue. Determining an appropriate partition number, $L$, for the value range, is important. Insufficient partition (small $L$) may lead to the inability to separate significant features, while excessive partition (large $L$) results in increased computing and storage costs. Following the study by He et al. (2017), we set $L$ to 256 to strike a balance between accuracy and costs.

To quantify the similarity between two contour probabilities, we assess the similarity of their distributions. This involves scaling the likelihood values of each grid point within the contour probability, treating them as distributions with the grid point $g$ as a random variable. The process is

$$\widehat{L_X}\left(g; \Gamma_i\right) = \frac{L_X\left(g; \Gamma_i\right)}{\int_G L_X\left(g; \Gamma_i\right) dg}$$

where $G$ is the set of all grid points. The Jensen–Shannon divergence between contour probability distributions is calculated, resulting in a dissimilarity matrix $DSM$. Dissimilarity and similarity are relative, and the similarity matrix $SM$ can be obtained by $SM = 1 - DSM$. To obtain the dissimilarity curve $DSC$, we compute the column-wise mean of $DSM$ as

$$DSC(i) = \frac{1}{L} \sum_{j=1}^{L} DSM(i, j).$$

By employing the same step, we calculate the similarity curve $SC$. The $DSC$ provides an overview of the average dissimilarity between each contour probability and all other contour probabilities. Crests in the curve indicate the contour probabilities that exhibit the least similarity to the others, while troughs represent the most similar contour probabilities.

### 4.2. Non-uniform downsampling

To ensure the selection of the $S$ most representative samples from $L$ isovalues, we employ non-uniform downsampling based on the $DSC$. Uniform downsampling techniques may skip isovalues that reflect important features and select some isovalues with a high local similarity that contain redundant information. Drawing inspiration from Bruckner and Möller (2010), who proposed a method for selecting representative isosurfaces based on similarity, we design a downsampling approach, which involves the following two steps:

**Partitioning intervals based on the dissimilarity curve:** We calculate the total area between the $DSC$ and the $X$-axis and divide it by the desired number $S$ of representative samples. This yields the unit interval area. We then divide the range of isovalues into $S$ intervals, each with an equal area based on the unit interval area.

**Selecting key-isovalues:** We use $SC$ as the initial priority function for selecting each isovalue. We scan through all available intervals and choose the isovalue $r$ with the highest priority as the representative isovalue for its corresponding interval. Once $r$ is selected, we penalize the priority of all other isovalue samples $i$ based on their similarity to $r$ as

$$p_i = \frac{p_i}{1 + SM(r, i)}.$$

We mark the interval containing the selected sample $r$ as unavailable and proceed to the next scan until $S$ isovalues are selected.

From a global perspective, the above downsampling approach prioritizes more sampling in intervals characterized by higher dissimilarity, thereby ensuring the selection of a greater number of unique contour structures. Within each interval, the most representative sample is chosen. Furthermore, the inclusion of penalization measures reduces the likelihood of selecting samples that can be adequately represented by already selected samples, while increasing the probability of selecting distinct contour structures.

### 4.3. Determination of sampling number

It is important to minimize the sampling number $S$ while ensuring information quality to reduce sampling of redundant isovalues and to increase the selection efficiency.

Firstly, we need to quantify the information loss associated with different sampling numbers. We adopt the information loss calculation method proposed by Zhou and Chiang (2018), which measures the difference between the interpolated reconstructed data after downsampling and the original data. Assuming isovalue $i$ and isovalue $j$ are selected while skipping the isovalues in between, the information loss can be calculated as

$$Loss(i, j) = \sum_{i<r<j} Diff_r = \sum_{i<r<j} \text{RMSE}\left(c_r; c_r'\right)$$

where $c_r'$ is the contour probability obtained by interpolating $c_i$ and $c_j$, and RMSE represents the root mean square deviation. By computing the information loss for all skipped isovalues, we obtain the total information loss

$$Loss_{total} = \sum_{\text{r is skipped}} Diff_r.$$

Here, we assume that the first and last samples are always selected for interpolating and reconstructing all the skipped isovalues.

Next, we iterate $S$ from 3 to $L/2$ and obtain the information loss curve. With each increase in sampling number, the

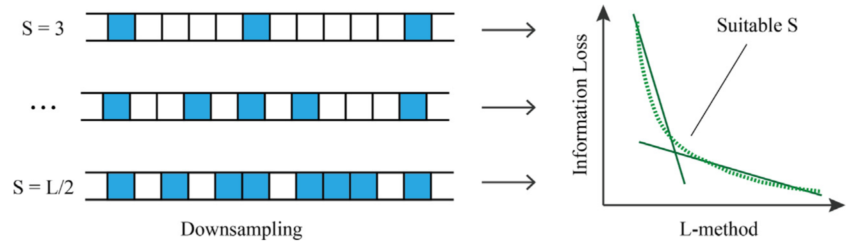


**Fig. 4.** Determination of sampling number. The correspondence between information loss and sampling number is plotted as a curve, and the appropriate sampling number is determined using the L-method.

downsampling algorithm selects a sample aiming to maximize information gain. The information loss curve exhibits an initial sharp decrease followed by a leveling off, resembling the shape of the letter L. To determine the optimal sampling number, we employ the L-method (Salvador and Chan, 2004). This method fits two straight lines to approximate the L-shaped curve, and the intersection of these lines indicates the turning point where the curve transitions from a steep decrease to a flattening trend. This turning point determines the appropriate sampling number, $S$, as illustrated in Fig. 4.

### 4.4. Visualization

We extract the ensemble isocontours corresponding to the selected $S$ key-isovalues to construct spaghetti plots. The spaghetti plot provides visual information regarding the geometric structure, spatial distribution, and variability range of the ensemble isocontours, assisting users in selecting key-isovalues.

The specific procedure for constructing the spaghetti plots is as follows: To ensure the visual effect of the spaghetti plot, each plot only displays $R$ isovalues, resulting in a set of spaghetti plots. For instance, when $S = 30$ and $R = 10$, we obtain three $(S/R)$ plots where the plot $i$ displays the ensemble isocontours corresponding to isovalues $\{0+i, 3+i, \ldots, 27+i\}$. Based on experimental trials and expert suggestions, we set $R = 10$ when $S > 30$ and $R = S/3$ when $S < 30$. Different ensemble isocontours are distinguished using a predefined set of color encodings. Since the spaghetti plot involves multiple visual elements overlapping with each other, interactive feedback is supported to convey specific information. When the user hovers the mouse cursor over a contour structure of interest, the corresponding ensemble isocontours will be highlighted, while the others will be grayed out. Additionally, a numerical tooltip will display the corresponding isovalue.

While ensemble mean and standard deviation plots have limitations in guiding the selection of isovalues, they can be used to understand the distribution of data and assess data quality. Therefore, we provide the ensemble mean and standard deviation plot alongside the spaghetti plots for users.

## 5. Hierarchical exploration visualization

As the size of ensemble members increases, the spaghetti plot suffers from significant visual clutter. To address this limitation, visual abstraction is commonly introduced. However, the drawback of visual abstraction is the loss of detailed information. To overcome visual clutter while still preserving the capability to explore isocontour details, we propose a hierarchical exploration of isocontour clusters visualization method based on agglomerative hierarchical clustering illustrated in Fig. 2(c).

In the following, we describe the agglomerative hierarchical clustering on ensemble isocontours extracted from selected isovalue, resulting in a binary hierarchical tree (Section 5.1). To accommodate ensemble isocontours with different dispersions and to optimize the interactive experience, we simplify the hierarchical tree based on specified parameters (Section 5.2). Subsequently, visual abstractions for isocontour clusters at each level are generated (Section 5.3), which are linked with a bubble tree to create the final visualization (Section 5.4).

### 5.1. Agglomerative hierarchical clustering

Given a set of 2D scalar fields $s_1^t, \ldots, s_N^t \in \mathbb{R}^M$ at a specific forecast time-step $t$, after confirming the isovalue, we extract the isocontours corresponding to the selected isovalue (i.e., the selected isocontours) from each ensemble member. To facilitate clustering and visual abstraction, we utilize the dead reckoning algorithm (Grevera, 2004) to compute the signed distance fields $d_1, \ldots, d_N \in \mathbb{R}^M$ for the selected isocontours. Each $d_i, i = 1, \ldots, N$ can be represented as a point in a high-dimensional Euclidean space $\mathbb{R}^M$.

Agglomerative hierarchical clustering is a commonly used method in visualizations involving line features, such as streamlines (Yu et al., 2012) and diffusion tensor imaging fiber bundles (Moberts et al., 2005). For constructing a cluster structure to enable hierarchical exploration of detailed information, we apply the agglomerative hierarchical clustering method proposed by Ferstl et al. (2016b,a) on the previous signed distance fields. Considering that variance is an important metric for meteorological experts to assess forecast uncertainty, we adopt Ward's method (Ward, 1963) in clustering to calculate the distance between clusters, specifically the increase in the sum of squared errors when two clusters are merged into one. We treated each signed distance field $d_i, i = 1, \ldots, N$ as an initial cluster and iteratively merged the two most similar clusters (i.e., the two clusters with the closest distance) until the total number of clusters met the stopping criterion.

The result of agglomerative hierarchical clustering is a binary hierarchical tree. At each non-leaf tree node, we record the inter-cluster distance between its two child nodes to simplify the hierarchical tree in subsequent steps.

### 5.2. Hierarchical tree simplification

Directly using the binary tree as a guide for hierarchical exploration, displaying only two isocontour clusters per level would increase the interaction cost for users to access information. Moreover, showing too many isocontour clusters per level can result in visual clutter. Therefore, determining the optimal number of isocontour clusters to display per level is a trade-off. This quantity is challenging to determine through quantitative calculations due to the uncertainty of subjective perception and the unpredictability of contour features.

Ensemble members tend to be more concentrated in the early forecast time, leading to overlapping clusters when displaying too many clusters. Conversely, in the late forecast time, ensemble members tend to be more dispersed, requiring the display of more clusters. Through in-depth discussions with meteorological experts, we have introduced two customizable parameters: the number of leaf node clusters $N_{cluster}$ and the number of branches per level $N_{branch}$ to simplify the hierarchical tree. Firstly, based on the recorded inter-cluster distances from the previous section, we iteratively merge the closest leaf nodes of the hierarchical tree to achieve the desired $N_{cluster}$. Then, we traverse the binary hierarchical tree, iteratively replacing the non-leaf child nodes that have the farthest inter-cluster distance with their two child nodes, until the number of branches per level reaches $N_{branch}$. This process allows us to obtain a hierarchical tree with a controllable number of leaf nodes and branches at each level, which is more suitable for interactive exploration. The default values for $N_{cluster}$ and $N_{branch}$ are set to 25% of the total number of ensemble members and 3, respectively.

### 5.3. Generation of visual abstractions

To abstractly summarize isocontour clusters and convey visual information about variability, we utilize a smooth isocontour band visual element created by merging the signed distance fields within each cluster.

Literature (Ferstl et al., 2016b) derived a generation method for the visual abstraction of isocontour clusters based on the Gaussian model. For cluster $k$, we calculate the mean $\mu_k \in \mathbb{R}^M$ and the diagonal of covariance matrix $\Sigma_k \in \mathbb{R}^{M\times M}$ of the signed distance field to generate an abstract isocontour band

$$B_k = \mathrm{CMIN}\left\{-\left(\mu_k - \alpha\sqrt{\mathrm{DIAG}\left(\Sigma_k\right)}\right), \mu_k + \alpha\sqrt{\mathrm{DIAG}\left(\Sigma_k\right)}\right\}$$

where $\alpha$ is the scaling factor that controls the width of the contour band and is set to 1. The CMIN operator represents the minimum operation applied to each grid point, while DIAG represents the diagonal operation. The resulting $B_k \in \mathbb{R}^M$ is a scalar field with $M$ grid points. In $B_k$, the isocontour corresponding to isovalue 0 is the mean isocontour, values greater than 0 represent the interior of the isocontour band, and values smaller than 0 represent the exterior of the isocontour band.

### 5.4. Visualization

We visualize the isocontour bands that represent the structure of each level in the hierarchical clustering tree. We utilize a bubble tree to provide an overview of the hierarchical distribution of ensemble isocontours. We link the bubble tree and the isocontour bands to facilitate interactive exploration of isocontour clusters at different levels or the original isocontours.

To obtain the visual abstraction element of the isocontour band, we apply a color mapping to the interior region of the isocontour band and emphasize the color representation of the mean isocontour.

In terms of the hierarchical tree, effectively conveying information about the clustering hierarchy is crucial for efficient hierarchical exploration (Gortler et al., 2018). Various visualization techniques have been developed to represent hierarchical structures, which can be categorized as explicit or implicit (Schulz et al., 2011). Explicit methods, such as node-link diagrams, illustrate the hierarchy through nodes connected by edges. On the other hand, implicit methods focus more on displaying the nodes and the information they carry, representing the hierarchy through encapsulation relationships, such as treemaps. In this paper, since we need to represent the size of tree nodes to reflect the number of ensemble members they contain, we choose an implicit method. However, treemap layouts can be too compact, leading to challenges in interaction and decreased interpretation effect of the hierarchical structure. Hence, we utilize the bubble tree visualization (Gortler et al., 2018), which strikes a balance between layout compactness and the interpretation effect of the hierarchy, while also facilitating hierarchical interaction.

Fig. 5 illustrates the visual encoding of the bubble tree. Circular bubbles represent the leaf nodes of the hierarchical tree, with their encapsulation relationships indicating the hierarchical structure. The color of the bubbles encodes the classification information of the isocontour clusters, using the same color scheme as the visual abstraction element of the isocontour band. The size of the bubbles encodes the number of ensemble members contained in the leaf node clusters, reflecting the probability information of the corresponding forecasts as indicated by Molteni et al. (1996).

We provide support for flexible switching to any level by clicking on the blank area of the bubble tree. When a level is selected, the leaf node bubbles contained will be highlighted, while the rest will be grayed out. As the levels are switched on the bubble tree, the visual abstraction of isocontour clusters at that level will be reconstructed. We establish a link between the two views by ensuring consistency in color channels and hierarchical relationships between the isocontour clusters and the bubble tree. To preserve the details of the isocontours, the isocontour band view directly displays the original isocontours when the user clicks on a leaf node bubble.

We choose to switch levels through the bubble tree instead of directly clicking on the clusters in the isocontour band view. The bubble tree provides an overview of the hierarchical structure, allowing users to switch to any level, rather than being limited to adjacent levels. The highlighted portion also helps users understand the position of the current cluster level as a whole. Furthermore, the isocontour band alone cannot convey the number of ensemble members it contains, whereas the bubble tree provides this additional information. By utilizing the hierarchical interaction of the bubble tree and the synchronized switching of the isocontour band view, users can progressively explore both the overall trend and the detailed distribution of isocontours.

## 6. Evaluation

To evaluate the utility, effectiveness, and usability of our method, we conducted case studies, quantitative assessments, and expert evaluations using real-world weather forecast data. The data was sourced from the TIGGE archive (Swinbank et al., 2016), which is commonly utilized in ensemble forecasting studies. Specifically, we utilize ensemble data of the geopotential height field at 500 hPa, consisting of 50 perturbed members. Our sample region covers 9° E to 160° E and 3° N to 85° N, with a spatial resolution of 0.5° × 0.5°. The forecast used in this paper starts at 16:00 UTC 18 January 2019. The closest work to ours is proposed by Ma and Entezari (2019), which has significant differences as discussed in Section 1. It offers limited support for isovalue selection, whereas our method samples a small number of representative isovalues from all optional isovalues, reducing the burden on users to navigate through numerous options. For visualization, our bubble tree offers both an overview and detailed exploration of multiple cluster levels, compared to the mode plot. Additionally, we mitigate the visual clutter of the spaghetti plot they adopt by integrating the confidence band. Thus, we decided to evaluate the core aspects of our method and reflect the benefits of these improvements in our evaluation.

### 6.1. Case studies

To demonstrate the practical application and the utility of our method, we conduct a series of experiments using the above weather forecast ensemble dataset. We select two representative cases for isovalue selection and isocontour exploration respectively. In the first case, we compare our method with uniform downsampling and ensemble mean and standard deviation

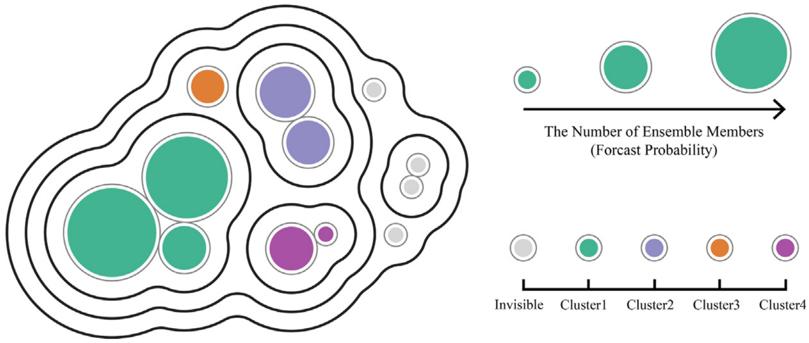


**Fig. 5.** Bubble tree and its visual encoding. Bubble encapsulation relationships indicate hierarchical structure, size indicates forecast probability, and color indicates clusters of different isocontours at the current level.

plots to validate its capability in selecting more comprehensive and accurate structural features of key contours. In the second case, we apply the hierarchical exploration visualization to c data with varying dispersions to verify the utility of our method in obtaining and analyzing the variability information of isocontours.

### 6.1.1. Isovalue selection

We select the dataset with a forecast lead time of 180 h. The baseline methods used are the uniform downsampling spaghetti plot and the ensemble mean and standard deviation plot.

Applying the method proposed in Section 4 to the dataset, we obtain Fig. 6(a–c), named group-a. The L-method results in 30 key-isovalues, with each view displaying 10 sets of isocontours. Additionally, we extract 30 sets of isocontours using uniform downsampling on the same dataset, which yielded Fig. 6(d–f), named group-b. The construction of group-b views follows the same approach as group-a, with adjacent three isovalues displayed in three views. A comparison between these two groups of views reveals that group-b's isocontours are more concentrated in the northern region, resulting in excessive rendering and visual clutter due to intersecting and interfering isocontours. In contrast, group-a presents fewer isocontours in the northern region but displays more discernible structural features, such as E1, E3, and E5. Most of the structures depicted by group-b in the northern region can be inferred from the limited structures in group-a, indicating redundant information in group-b. Moreover, group-a depicts more contour structures in the southern region, specifically for features E2 and E4, displaying more isocontours in all three views compared to group-b. On the other hand, feature E6 represents a fragmented part of the blue isocontour set, and feature E7 represents a portion of the green isocontour set, but they are difficult to identify in group-b.

Traditionally, the ensemble mean and standard deviation plots are used to guide users in selecting isovalues. Fig. 7 illustrates the mean and standard deviation plot created using the same data. The mean of ensemble members is mapped as isocontours, while the standard deviation of ensemble members' values at each grid point is represented by the background color. Users typically select isovalues based on the amount of high standard deviation regions crossed by the isocontours. However, in regions with steep gradients, even small displacements can lead to large standard deviations, making it challenging to fully represent the variability of the isocontours using this approach. For instance, region E1 in Fig. 7(a) exhibits a high standard deviation, but the range of variability for the isocontours in the same position in Fig. 7(b) is smaller. In the E2 region of Fig. 7(b), the purple isocontours demonstrate greater variability, whereas this variation is not easily observed in the same position in Fig. 7(a). These limitations hinder meteorological experts from effectively selecting key-isovalues based on the variability of isocontours. In contrast, our method provides intuitive visual guidance for isovalue selection while minimizing information loss.

### 6.1.2. Isocontours exploration

To illustrate the exploration of isocontours under different variabilities, we selected datasets with an isovalue of 5412 m and forecast lead times of 180 h and 60 h.

For the 180 h forecast lead time, the isocontours exhibit higher dispersion. We set $N_{cluster} = 12$ and $N_{branch} = 3$ to obtain Fig. 8(a–b). Fig. 8(a) shows the structure of isocontour clusters at the first level of the hierarchical tree. It includes three clusters represented by different colors: orange, purple, and green. The orange and purple clusters represent the two major trends, while the green cluster represents the outlier. During the hierarchical clustering process, the outlier data points are merged into clusters at a later stage, allowing users to quickly identify outlier isocontours initially. By comparing the number and size of the orange and purple bubbles, we can conclude that the orange cluster contains more ensemble members than the purple cluster, indicating a higher likelihood of the isocontour corresponding to isovalue 5412 m being distributed in the vicinity of the orange cluster. With this view, users can easily capture the differences between the orange and purple clusters, mainly concentrated in region A. Once users understand the spatial distribution within each cluster and the differences between clusters, they can click on the corresponding hierarchy structure in the bubble tree to switch to any branch of interest. In this case, the user selects the orange cluster to further explore the details. Fig. 8(b) shows that this cluster is divided into three finer-grained clusters, with the green cluster exhibiting significant differences from the orange and purple clusters in region B. The green cluster is located further north in region B. These detailed differences are not easily discernible in the visual abstraction of Fig. 8(a) but become apparent after user interaction.

For the 60 h forecast lead time, the isocontours exhibit higher concentration. We set $N_{cluster} = 6$ and $N_{branch} = 2$ to obtain Fig. 8(c–d). Fig. 8(c) and Fig. 8(d) depict the variability of isocontours when ensemble members have lower dispersion at an earlier forecast time. At this time, there are major differences in the purple and green clusters only in region C. Compared to the 180 h forecast, although representing the isocontour corresponding to the same isovalue, the spatial variability range narrows, and the distribution becomes more concentrated. This indicates lower uncertainty and higher confidence in the forecast.

The above analysis results demonstrate that the interactive visualization method designed in this paper effectively supports users in obtaining detailed differences, variability ranges, major trends, and outliers in ensemble isocontours.

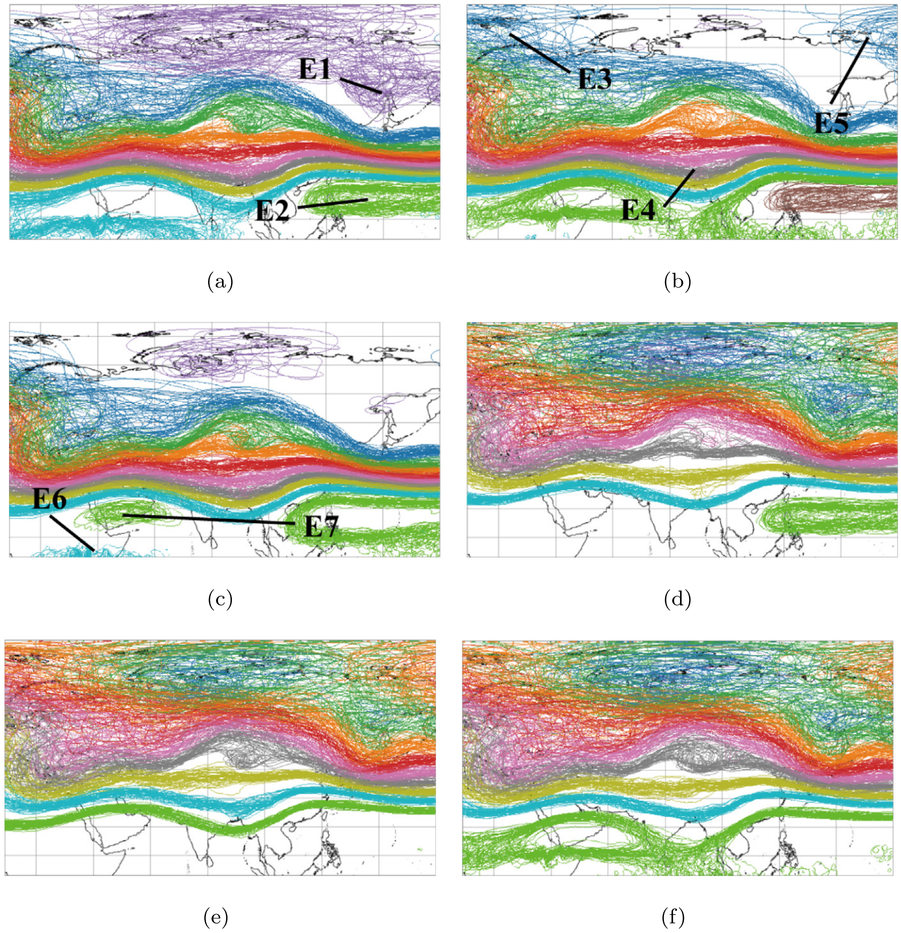


**Fig. 6.** Comparison of our method (a–c) and uniform downsampling (d–f) for isovalue selection. The isocontours are from the geopotential height field at 500 hPa of the TIGGE dataset.

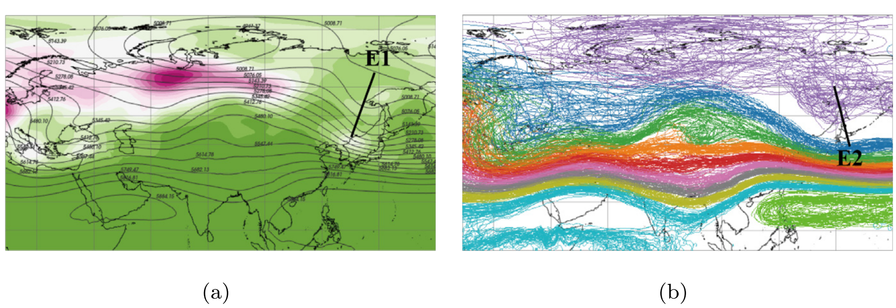


**Fig. 7.** Analogous to Fig. 6. Comparison of the ensemble mean and standard deviation plots (a) and our method (b) for isovalue selection.

### *6.2. Quantitative assessments*

This section provides quantitative assessments of the effectiveness of our method in terms of information loss and visual clutter. We begin with the experimental results of downsampling calculation and information loss curve to validate the capability of our method in selecting key-isovalues while controlling information loss. Subsequently, we compare and evaluate the spaghetti plot with our method to verify its capability to overcome visual clutter.

#### *6.2.1. Downsampling results and information loss curve*

To analyze the characteristics of the proposed key-isovalue selection method, we perform calculations on the downsampling results and information loss curve using the data from Section 6.1.1, as illustrated in Fig. 9. The downsampling results provide insights into the relationship between the selected isovalues, the sampling number, and the dissimilarity of isovalues. On the other hand, the information loss curve demonstrates the extent to which the isocontours corresponding to the selected isovalue preserve the original ensemble contour features. Fig. 9(a) illustrates the isovalue selection under different sampling numbers. Certain isovalues are consistently selected across various sampling numbers, indicating their representativeness and importance. The information loss, as shown in Fig. 9(b), exhibits an initial sharp decrease followed by a gradual decline. This indicates that our downsampling method achieves significant gains with each additional sampling number. Fig. 9(b) also demonstrates the result of the L-method, with two straight lines fitted to the curve, determining the optimal sampling number as 30.

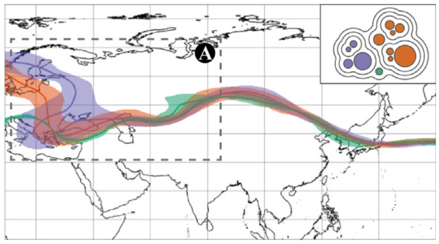

(a) 180 h, $N_{cluster} = 12$, $N_{branch} = 3$

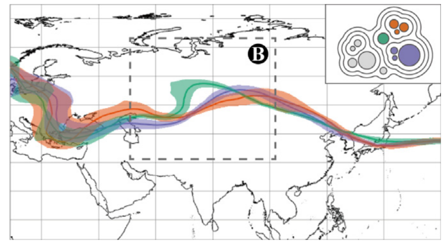

(b) 180 h, $N_{cluster} = 12$, $N_{branch} = 3$

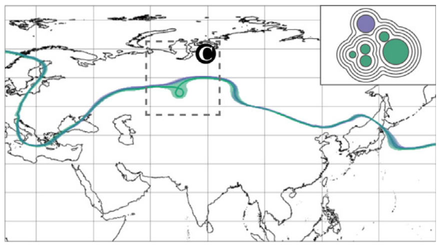

(c) 60 h, $N_{cluster} = 6$, $N_{branch} = 2$

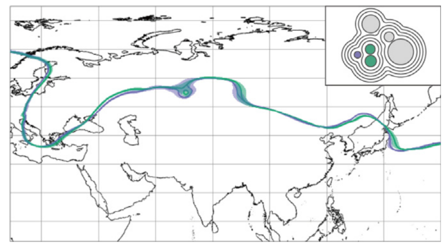

(d) 60 h, $N_{cluster} = 6$, $N_{branch} = 2$

**Fig. 8.** Hierarchical exploration visualization of an ensemble of 5412 m geopotential height isocontours at 500 hPa. When the time-steps are 180 h (a–b) and 60 h (c–d), respectively, we used different hierarchy parameters for plotting.

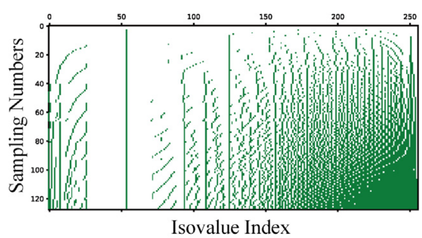


(a)

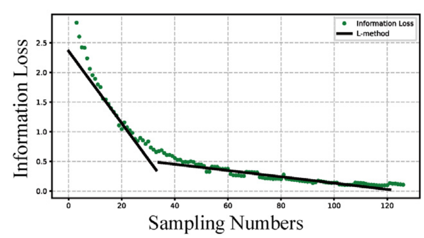


(b)

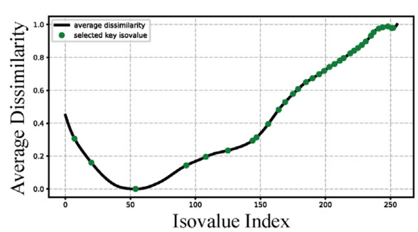


(c)

**Fig. 9.** Isovalue selection (a) and information loss (b) with different sampling numbers and average dissimilarity curve (c) for the example shown in Fig. 6.

This number is considerably smaller than the initial 256 isovalues in the value range. In Fig. 9(c), the dissimilarity curve is displayed, with green dots highlighting the isovalues that are finally sampled. The distribution of these green dots reveals a nonlinear sampling process. More isovalues are selected in regions with higher dissimilarity, allowing for the inclusion of more unique isocontours. Within each local region, the most similar points are chosen, effectively representing the nearby isocontours. Fig. 9(a) and Fig. 9(c) exhibit shape consistency because the dissimilarity curve indicates the uniqueness of the isocontours, and the probability of selection aligns with this curve. By selecting representative key-isovalues based on the determined optimal sampling number, we achieve control over information loss. The visual information of the isocontours corresponding to these key-isovalues is presented to guide users in their selections.

*6.2.2. Visual clutter of isocontour exploration*

Current literature (Sanyal et al., 2010; Ferstl et al., 2016b; Whitaker et al., 2013; Zhang et al., 2023) overcome the visual clutter in spaghetti plots by employing visual abstractions. However, none of these studies have quantitatively assessed the effectiveness of overcoming visual clutter, particularly when multiple abstract visual elements are superimposed and challenged by the increasing size of ensemble forecast members. To solve this problem, we adopt the Feature Congestion measure proposed by Rosenholtz et al. (2007) to comparatively and quantitatively assess the visual clutter of spaghetti plots and our method under different numbers of ensemble members using the data from Section 6.1.2.

To evaluate the visual clutter, we progressively increased the number of ensemble members from 1 to 51, adding 2 members at a time. We generated two groups, each containing 26 views,

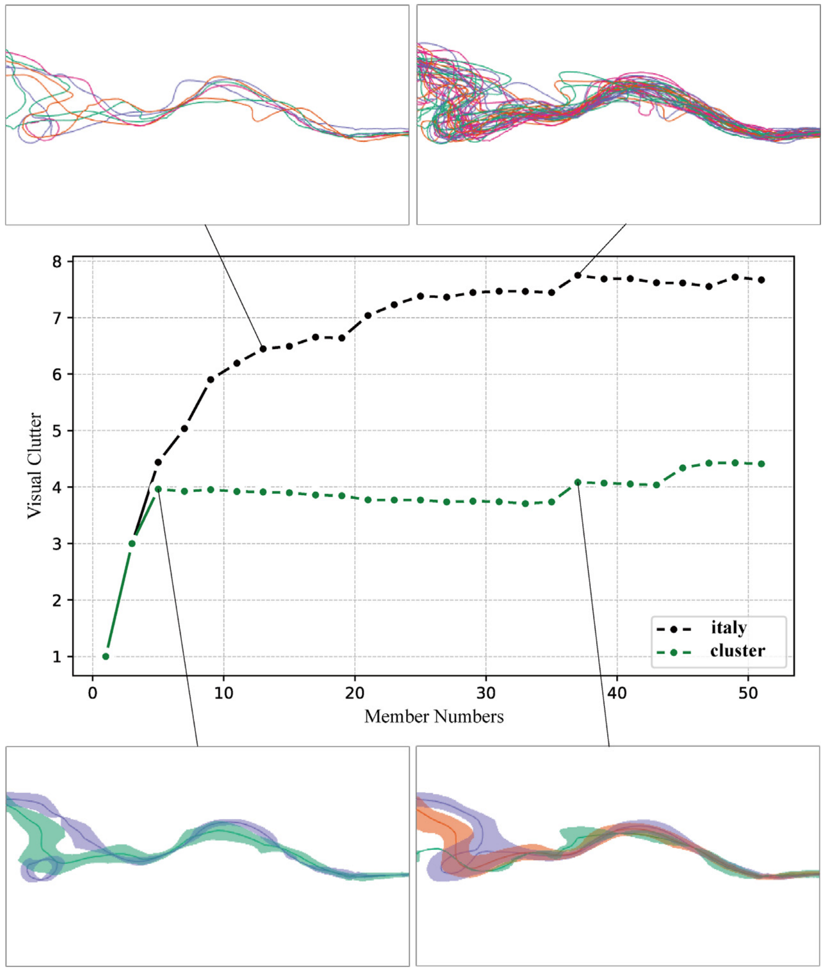


**Fig. 10.** Comparison of the visual clutter of our method (bottom) and the spaghetti plot (top) with different sizes of ensemble members.

named group-italy and group-cluster. Both groups removed the background to avoid interference. In the group-cluster, the 51 ensemble members are pre-clustered into 4 clusters, and the corresponding visual elements are drawn during the view generation process based on the currently involved ensemble members, avoiding re-clustering for each additional member. The views in the group-cluster may contain 1 to 4 clusters; if a cluster does not have any participating members, it is not displayed.

Fig. 10 presents the results of the quantitative assessment. The visual clutter in the group-cluster is significantly lower compared to group-italy. As the size of ensemble members increases, the visual clutter in group-italy continues to rise, while the group-cluster remains relatively stable, with only a slight increase when a new cluster appears in the view. Another interesting observation is that the rate of increase in visual clutter slows down for group-italy as the size of ensemble members further increases. This can be attributed to the fact that with more overlap isocontours, the problem of overplotting becomes more severe. Visually, the overplotted view tends to be perceived as a texture with scattered dots, making it challenging for observers to interpret the geometric structure of the isocontours. Overall, these findings validate the effectiveness of our visualization method in overcoming visual clutter.

### *6.3. Expert evaluation*

We conduct in-depth open-ended interviews with 8 experts (3 females and 5 males, with an average experience of 13.6 years) from the meteorological industry. These interviews aim to gather their feedback on our approach, confirm its usability, and identify potential application scenarios. Among them, three experts (P1–P3) are involved in the method design process in Section 3, while other experts (P4–P8) use our method for the first time. P4 is a senior engineer with 8 years of experience in weather forecast system development. Both P5 and P6 are forecasters who frequently use weather forecast visualization tools with 9 and 15 years of experience, respectively. P7 and P8 are meteorologists specializing in climatology for 12 and 18 years, respectively.

During the interviews, we first provide a brief overview of our research background and focus to the experts. We then demonstrate the usage process and visual design of our method using the two case studies presented in Section 6.1. Next, experts are asked to freely explore the data described in Section 6 using our method, with encouragement to share their thoughts and opinions during the exploration process, which is collected by us.

In general, the experts highly praise our method, particularly in isovalue selection and interactive isocontour exploration, as they recognize its relevance to practical meteorological work. We summarize their feedback in the following three aspects.

**Method design:** The experts find the visualization design of our method to be intuitive and easy to understand and use. Despite introducing a new visual abstraction element, the isocontour band, it remains consistent with their previous experience using spaghetti plots. Expert P5 comments on the transferability of usage experience, *"Common ensemble forecast platforms currently* *provide visual tools like spaghetti plots and ensemble mean and standard deviation plots, making it easy for meteorological professionals to transfer their usage experience to this method."* Expert P2 highlights the value of the design from a visualization perspective, *"The design, whether downsampling or visual abstraction, essentially presents a subset of the most valuable information when the information overload exceeds the user's capacity, thereby stimulating further exploration. We often adopt this approach when designing other visualization methods. The key is to determine what is the most valuable information for the user, and this method does a good job of that based on meteorological expert needs."* Expert P4 adds, *"There is a strong correlation between key-isovalue selection and hierarchical exploration visualization, which can form a more complete workflow and have practical value."* Expert P6 proposes an improvement, *"The current method requires the manual setting of two hierarchical structure parameters to handle isocontours with different dispersions. In the future, it can be enhanced to automatically generate these parameters."*

**Method usability:** Expert P3 comments on isovalue selection, *"This method selects key-isovalue based on the uniqueness and representativeness of the contour structure corresponding to those isovalues, which is reasonable and effective. This is particularly true in scenarios where prior knowledge about specific isovalues is lacking."* Expert P7 expresses a keen interest in interactive hierarchical exploration visualization, believing that it could help overcome the limitations of existing visualization tools when dealing with a large size of ensemble members. This feature facilitates the observation and analysis of differences in isocontours among different forecast members. Expert P1 notes, *"This visualization method helps forecasters interpret ensemble forecast products and can be used in conjunction with other visualization applications currently deployed by meteorological administration to create user-friendly products for forecasters."* They express hope that this visualization method could be deployed and tested in meteorological administration, suggesting further collaboration. Expert P8 proposes, *"In fact, this visualization method can also be applied to other studies, such as streamline visualization of wind fields and visualization of typhoon paths. It can be considered to extend this method from a broader research perspective beyond isocontours."*

**Application scenarios**: Through discussions with domain experts, we identify several valuable application scenarios for our visualization method. These include: (1) Assisting meteorological professionals in observing isocontours of subtropical high, isohyets, and isotherms, and combining them with other tools to explain the uncertainty of weather forecasts for high temperatures, droughts, and heavy rainfall. (2) Enabling meteorological professionals to analyze the influence of specific topography, such as the Qinghai-Tibet Plateau, on the trends of various isocontours. (3) Assisting meteorological professionals in comparing the specific spatial distribution differences among ensemble forecast members, evaluating the predictive performance of each member based on historical data, and reconstructing forecasts by selecting optimal members or integrating various products to improve the performance of ensemble forecasts. In these scenarios, our proposed method can help meteorological professionals visually and comprehensively observe and explore the features of various isocontours in ensemble data, supporting further analysis by combining their domain expertise with other statistical analysis tools.

## 7. Discussion

Although the utility, effectiveness, and usability of the proposed method have been validated in our evaluation, there are still some limitations in this paper considering the challenges of ensemble data visualization. Based on the evaluation results, we believe there is room for improvement in the following two aspects:

**Contour probability similarity:** Considering computational efficiency, we used Jensen–Shannon divergence to calculate the similarity of contour probabilities. However, when two probability distributions have no overlap, the Jensen–Shannon divergence becomes a constant. Therefore, for regions with smaller contour variations, the computed similarity may differ from the perceived similarity by the human eye. In the future, we plan to strike a balance between computational efficiency and similarity accuracy by developing a similarity measure that aligns more closely with human intuition, while still maintaining an acceptable computational cost. This will contribute to the improvement of the above situation.

**Visual channel of isocontour bands**: When exploring the hierarchical structure of isocontour clusters, the color channel changes with different levels of isocontour bands, which requires users to adapt to the new visual information. In the future, we plan to implement smooth animation interpolation using signed distance fields. Additionally, the overlapping of isocontour bands leads to color blending, making it challenging for users to distinguish between different clusters. We plan to scatter pixels in the overlapping regions with the same color as their respective clusters, thus enhancing their discriminability.

## 8. Conclusion

In this paper, we propose a novel approach to achieve key-isovalue selection guided by contours and hierarchical exploration of isocontour clusters in 2D scalar field ensembles. Our method involves extracting contour probabilities for each median isovalue by partitioning the value range of the scalar field. We then perform non-uniform downsampling based on the similarity of these contour probabilities to select representative samples of isocontours. This guides users in isovalue selection. Simultaneously, we automatically determine the optimal downsampling number using an information loss curve, ensuring a balance between selection efficiency and information preservation. To construct visual abstractions of isocontour clusters, we introduce a novel visualization based on agglomerative hierarchical clustering. It allows for flexible switching between different levels of visual abstraction, enabling users to explore detailed information. By balancing the conflicting requirements of summarization of visual abstraction and preservation of detailed information, our approach provides an intuitive understanding of the variability evolution of weather forecast ensembles. Our case studies, quantitative assessments, and expert evaluations reveal the utility, effectiveness, and usability of our approach. In future work, we plan to extend our method from analyzing ensemble isocontours at individual time points to analyzing the temporal evolution of ensemble isocontours over a period suggested by our expert participants. This extension will enhance the applicability of our approach and enable a more comprehensive analysis of the uncertainty and confidence of ensemble isocontours.

## CRediT authorship contribution statement

**Feng Zhou:** Writing – review & editing, Writing – original draft, Visualization, Validation, Supervision, Software, Resources, Methodology, Investigation, Data curation, Conceptualization. **Hao Hu:** Methodology, Investigation, Data curation, Conceptualization. **Fengjie Wang:** Writing – review & editing, Investigation, Conceptualization. **Jiamin Zhu:** Writing – review & editing, Investigation, Conceptualization. **Wenwen Gao:** Writing – review & editing. **Min Zhu:** Writing – review & editing, Methodology, Investigation, Conceptualization.

## Ethical approval

This study does not contain any studies with Human or animal subjects performed by any of the authors.

## Declaration of competing interest

The authors declare that they have no known competing financial interests or personal relationships that could have appeared to influence the work reported in this paper.

## References


Bruckner, S., Möller, T., 2010. Isosurface similarity maps. Comput. Graph. Forum 29 (3), 773–782. http://dx.doi.org/10.1111/j.1467-8659.2009.01689.x.

De Souza, C.V.F., Bonnet, S.M., De Oliveira, D., Cataldi, M., Miranda, F., Lage, M., 2023. ProWis: a visual approach for building, managing, and analyzing weather simulation ensembles at runtime. IEEE Trans. Vis. Comput. Graphics 1–10. http://dx.doi.org/10.1109/TVCG.2023.3326514.

Ferstl, F., Burger, K., Westermann, R., 2016a. Streamline variability plots for characterizing the uncertainty in vector field ensembles. IEEE Trans. Vis. Comput. Graphics 22 (1), 767–776. http://dx.doi.org/10.1109/TVCG.2015.2467204.

Ferstl, F., Kanzler, M., Rautenhaus, M., Westermann, R., 2016b. Visual analysis of spatial variability and global correlations in ensembles of iso-contours. Comput. Graph. Forum 35 (3), 221–230. http://dx.doi.org/10.1111/cgf.12898.

Ferstl, F., Kanzler, M., Rautenhaus, M., Westermann, R., 2017. Time-hierarchical clustering and visualization of weather forecast ensembles. IEEE Trans. Vis. Comput. Graphics 23 (1), 831–840. http://dx.doi.org/10.1109/TVCG.2016.2598868.

Gortler, J., Schulz, C., Weiskopf, D., Deussen, O., 2018. Bubble treemaps for uncertainty visualization. IEEE Trans. Vis. Comput. Graphics 24 (1), 719–728. http://dx.doi.org/10.1109/TVCG.2017.2743959.

Grevera, G.J., 2004. The "dead reckoning" signed distance transform. Comput. Vis. Image Underst. 95 (3), 317–333. http://dx.doi.org/10.1016/j.cviu.2004.05.002.

Hazarika, S., Biswas, A., Dutta, S., Shen, H.-W., 2018. Information guided exploration of scalar values and isocontours in ensemble datasets. Entropy 20 (7), 540. http://dx.doi.org/10.3390/e20070540.

He, W., Liu, X., Shen, H.-W., Collis, S.M., Helmus, J.J., 2017. Range likelihood tree: a compact and effective representation for visual exploration of uncertain data sets. In: 2017 IEEE Pacific Visualization Symposium. PacificVis, IEEE, Seoul, South Korea, pp. 151–160. http://dx.doi.org/10.1109/PACIFICVIS.2017.8031589.

Kamal, A., Dhakal, P., Javaid, A.Y., Devabhaktuni, V.K., Kaur, D., Zaientz, J., Marinier, R., 2021. Recent advances and challenges in uncertainty visualization: a survey. J. Vis. 24 (5), 861–890. http://dx.doi.org/10.1007/s12650-021-00755-1.

Kumpf, A., Rautenhaus, M., Riemer, M., Westermann, R., 2019. Visual analysis of the temporal evolution of ensemble forecast sensitivities. IEEE Trans. Vis. Comput. Graphics 25 (1), 98–108. http://dx.doi.org/10.1109/TVCG.2018.2864901.

Kumpf, A., Tost, B., Baumgart, M., Riemer, M., Westermann, R., Rautenhaus, M., 2018. Visualizing confidence in cluster-based ensemble weather forecast analyses. IEEE Trans. Vis. Comput. Graphics 24 (1), 109–119. http://dx.doi.org/10.1109/TVCG.2017.2745178.

Leutbecher, M., Palmer, T., 2008. Ensemble forecasting. J. Comput. Phys. 227 (7), 3515–3539. http://dx.doi.org/10.1016/j.jcp.2007.02.014.

Liu, L., Boone, A.P., Ruginski, I.T., Padilla, L., Hegarty, M., Creem-Regehr, S.H., Thompson, W.B., Yuksel, C., House, D.H., 2017. Uncertainty visualization by representative sampling from prediction ensembles. IEEE Trans. Vis. Comput. Graphics 23 (9), 2165–2178. http://dx.doi.org/10.1109/TVCG.2016.2607204.

Liu, L., Padilla, L., Creem-Regehr, S.H., House, D.H., 2019. Visualizing uncertain tropical cyclone predictions using representative samples from ensembles of forecast tracks. IEEE Trans. Vis. Comput. Graphics 25 (1), 882–891. http://dx.doi.org/10.1109/TVCG.2018.2865193.

Ma, B., Entezari, A., 2019. An interactive framework for visualization of weather forecast ensembles. IEEE Trans. Vis. Comput. Graphics 25 (1), 1091–1101. http://dx.doi.org/10.1109/TVCG.2018.2864815.

Mirzargar, M., Whitaker, R.T., Kirby, R.M., 2014. Curve boxplot: generalization of boxplot for ensembles of curves. IEEE Trans. Vis. Comput. Graphics 20 (12), 2654–2663. http://dx.doi.org/10.1109/TVCG.2014.2346455.

Moberts, B., Vilanova, A., van Wijk, J., 2005. Evaluation of fiber clustering methods for diffusion tensor imaging. In: VIS 05. IEEE Visualization, 2005. pp. 65–72. http://dx.doi.org/10.1109/VISUAL.2005.1532779.

Molteni, F., Buizza, R., Palmer, T.N., Petroliagis, T., 1996. The ECMWF ensemble prediction system: methodology and validation. Q. J. R. Meteorol. Soc. 122 (529), 73–119. http://dx.doi.org/10.1002/qj.49712252905.

Obermaier, H., Joy, K.I., 2014. Future challenges for ensemble visualization. IEEE Comput. Graph. Appl. 34 (3), 8–11. http://dx.doi.org/10.1109/MCG.2014.52.

Pfaffelmoser, T., Westermann, R., 2012. Visualization of global correlation structures in uncertain 2D scalar fields. Comput. Graph. Forum 31 (3pt2), 1025–1034. http://dx.doi.org/10.1111/j.1467-8659.2012.03095.x.

Pothkow, K., Hege, H.-C., 2011. Positional uncertainty of isocontours: condition analysis and probabilistic measures. IEEE Trans. Vis. Comput. Graphics 17 (10), 1393–1406. http://dx.doi.org/10.1109/TVCG.2010.247.

Pöthkow, K., Hege, H.-C., 2013. Nonparametric models for uncertainty visualization. Comput. Graph. Forum 32 (3pt2), 131–140. http://dx.doi.org/10.1111/cgf.12100.

Quinan, P.S., Meyer, M., 2016. Visually comparing weather features in forecasts. IEEE Trans. Vis. Comput. Graphics 22 (1), 389–398. http://dx.doi.org/10.1109/TVCG.2015.2467754.

Rautenhaus, M., Bottinger, M., Siemen, S., Hoffman, R., Kirby, R.M., Mirzargar, M., Rober, N., Westermann, R., 2018. Visualization in meteorology–a survey of techniques and tools for data analysis tasks. IEEE Trans. Vis. Comput. Graphics 24 (12), 3268–3296. http://dx.doi.org/10.1109/TVCG.2017.2779501.

Rosenholtz, R., Li, Y., Nakano, L., 2007. Measuring visual clutter. J. Vis. 7 (2), 17. http://dx.doi.org/10.1167/7.2.17.

Salvador, S., Chan, P., 2004. Determining the number of clusters/segments in hierarchical clustering/segmentation algorithms. In: 16th IEEE International Conference on Tools with Artificial Intelligence. IEEE Comput. Soc, Boca Raton, FL, USA, pp. 576–584. http://dx.doi.org/10.1109/ICTAI.2004.50.

Sanyal, J., Zhang, S., Dyer, J., Mercer, A., Amburn, P., Moorhead, R.J., 2010. Noodles: a tool for visualization of numerical weather model ensemble uncertainty. IEEE Trans. Vis. Comput. Graphics 16 (6), 1421–1430. http://dx.doi.org/10.1109/TVCG.2010.181.

Schulz, H.-J., Hadlak, S., Schumann, H., 2011. The design space of implicit hierarchy visualization: a survey. IEEE Trans. Vis. Comput. Graphics 17 (4), 393–411. http://dx.doi.org/10.1109/TVCG.2010.79.

Swinbank, R., Kyouda, M., Buchanan, P., Froude, L., Hamill, T.M., Hewson, T.D., Keller, J.H., Matsueda, M., Methven, J., Pappenberger, F., Scheuerer, M., Titley, H.A., Wilson, L., Yamaguchi, M., 2016. The TIGGE project and its achievements. Bull. Am. Meteorol. Soc. 97 (1), 49–67. http://dx.doi.org/10.1175/BAMS-D-13-00191.1.

Viola, I., Chen, M., Isenberg, T., 2020. Visual abstraction. Found. Data Vis. 15–37. http://dx.doi.org/10.1007/978-3-030-34444-3_2.

Wang, C., 2020. Representative isovalue detection and isosurface segmentation using novel isosurface measures. Comput. Graph. Forum 39 (3), 37–47. http://dx.doi.org/10.1111/cgf.13961.

Wang, J., Hazarika, S., Li, C., Shen, H.-W., 2019. Visualization and visual analysis of ensemble data: a survey. IEEE Trans. Vis. Comput. Graphics 25 (9), 2853–2872. http://dx.doi.org/10.1109/TVCG.2018.2853721.

Ward, J.H., 1963. Hierarchical grouping to optimize an objective function. J. Amer. Statist. Assoc. 58 (301), 236–244. http://dx.doi.org/10.1080/01621459.1963.10500845.

Whitaker, R.T., Mirzargar, M., Kirby, R.M., 2013. Contour boxplots: a method for characterizing uncertainty in feature sets from simulation ensembles. IEEE Trans. Vis. Comput. Graphics 19 (12), 2713–2722. http://dx.doi.org/10.1109/TVCG.2013.143.

Yu, H., Wang, C., Shene, C.-K., Chen, J.H., 2012. Hierarchical streamline bundles. IEEE Trans. Vis. Comput. Graphics 18 (8), 1353–1367. http://dx.doi.org/10.1109/TVCG.2011.155.

Zhang, M., Chen, L., Li, Q., Yuan, X., Yong, J., 2021. Uncertainty-oriented ensemble data visualization and exploration using variable spatial spreading. IEEE Trans. Vis. Comput. Graphics 27 (2), 1808–1818. http://dx.doi.org/10.1109/TVCG.2020.3030377.

Zhang, M., Li, Q., Chen, L., Yuan, X., Yong, J., 2023. Enconvis: a unified framework for ensemble contour visualization. IEEE Trans. Vis. Comput. Graphics 29 (4), 2067–2079. http://dx.doi.org/10.1109/TVCG.2021.3140153.

Zhou, B., Chiang, Y.-J., 2018. Key time steps selection for large-scale time-varying volume datasets using an information-theoretic storyboard. Comput. Graph. Forum 37 (3), 37–49. http://dx.doi.org/10.1111/cgf.13399.